Journal of Solid State Chemistry **160,** 108–117 (2001)
doi:10.1006/jssc.2001.9200, available online at http://www.idealibrary.com on IDEAL®

Topotactic Reactions, Structural Studies, and Lithium Intercalation in Cation-Deficient Spinels with Formula Close to $Li_2Mn_4O_9$

A. Ibarra Palos, M. Anne, and P. Strobel[1]

Laboratoire de Cristallographie, CNRS, BP 166, 38042 Grenoble Cedex 9, France

Received December 16, 2000; in revised form March 25, 2001; accepted April 9, 2001; published online June 15, 2001

The composition $Li_2Mn_4O_9$, reported as a spinel oxide containing vacancies on both tetrahedral and octahedral sites [A. de Kock *et al.*, *Mater. Res. Bull.* 25, 657 (1990)], was approached using three different preparation routes: low-temperature solid state reaction (A), chemical delithiation (B), and electrochemical delithiation (C). Rietveld refinements from neutron diffraction data confirmed the double-vacancy scheme proposed previously for product A, but with more tetrahedral and fewer octahedral vacancies than in the ideal $Li_2Mn_4O_9$ formula. Low-temperature solid state reactions systematically result in broad reflections. Sample B, which was obtained topotactically, exhibits much narrower reflections. But chemical analyses, thermogravimetry, and neutron diffraction show that the acid treatment introduces significant amounts of protons, resulting in a formula close to $Li_{0.92}HMn_4O_9$. Samples A and B were cycled electrochemically in lithium cells at 3 V with better stability than $LiMn_2O_4$, probably due to their higher initial manganese oxidation state. No separate electrochemical step linked to the filling of vacancies is observed in A, whereas B gives an additional redox step ca. 200 mV above the main plateau. This feature is not observed on compounds A or C; it is reversible, and seems to be a specific property of this spinel with a low initial cell parameter (8.09 Å). Sample A2 with double cation vacancies is especially stable on cycling at 3 V, and shows a very small volume variation on lithium intercalation.

Key Words: **Li–Mn–O system; spinel; cation vacancies; neutron diffraction; lithium intercalation.**

1. INTRODUCTION

The Li–Mn–O spinel system gives rise to a rich crystal chemistry and a wide interest due to its potential applications in lithium batteries (1–3). A range of stoichiometric compositions is known between the limiting compounds $LiMn_2O_4$ and $Li_4Mn_5O_{12}$, as well as phases containing tetrahedral site vacancies, such as λ-MnO_2. A very peculiar case in this system is $Li_2Mn_4O_9$, initially reported by de Kock *et al.* (4). This compound is interesting, because (i) it contains tetravalent manganese only and (ii) its structure contains cation vacancies on *both* tetrahedral and octahedral sites. From a neutron diffraction study, de Kock *et al.* indeed concluded the structural formula $(Li_{8/9}\square_{1/9})[Mn_{16/9}\square_{2/9}]O_4$ in spinel stoichiometry, where ( ) and [ ] indicate the tetrahedral and octahedral site contents, respectively. Such a high cation deficiency could lead to high lithium intercalation capacity, although the reversibility of intercalation in such sites is doubtful *a priori*.

The synthesis of $Li_2Mn_4O_9$, however, is difficult, and subsequent attempts by several groups (3, 5–7) to reproduce de Kock's result yielded products with a manganese oxidation state v(Mn) never exceeding $+3.85$, while this composition was cited in several recent works without any manganese oxidation state determination (8–10). In this work, we reconsider the $Li_2Mn_4O_9$ case, using three different preparation routes.

The stoichiometric issues considered here and their relevance to lithium intercalation can be conveniently illustrated using a composition–valence phase diagram, using as coordinate axes the Li/Mn ratio and the manganese oxidation state v(Mn) (11). In this representation (Fig. 1), lithium intercalation/extraction reactions follow parallel lines with slope -1, the length of which is directly proportional to the capacity in the case of an electrochemical intercalation/extraction process. In addition, v(Mn) is immediately visible for any composition. Figure 1 shows relevant compositions such as the stoichiometric spinel solution $Li_{1+\alpha}Mn_{2-\alpha}O_4$, with its limits $\alpha = 0$ ($LiMn_2O_4$) and $\alpha = 1/3$ ($Li_4Mn_5O_{12}$), typical compositions located in the cation-deficient range (λ-$MnO_2 = \square Mn_2O_4$, and $Li_2Mn_4O_9$), as well as the limit of occurrence of tetragonal distorsion of the spinel structure due to the Jahn-Teller cation Mn^{3+}.

De Kock *et al.* prepared "$Li_2Mn_4O_9$" by direct solid state reaction from MnO_2 and LiOH. Figure 1 shows that such a composition can be reached *topotactically*, by lithium extraction from a stoichiometric spinel belonging to the $Li_{1+\alpha}Mn_{2-\alpha}O_4$ line. The composition of this "parent

[1] To whom correspondence should be addressed. E-mail: strobel@labs.polycnrs-gre.fr.

0022-4596/01 $35.00

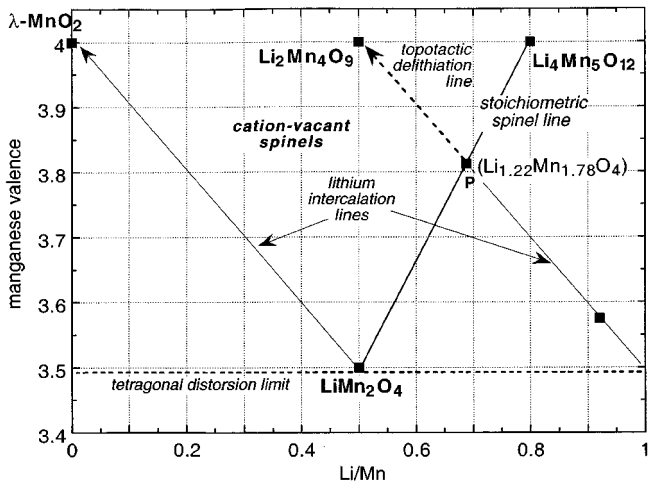

FIG. 1. Composition–valence phase diagram for the Li–Mn–O system. The expected topotactic lithium extraction yielding $Li_2Mn_4O_9$ starts from composition P (see text).

spinel" is simply determined by the condition Mn/O = 4/9, resulting in the initial formula $Li_{11/9}Mn_{16/9}O_4$ ($\alpha = 2/9$, point P in Fig. 1). However, lithium extraction is expected to occur preferentially from the tetrahedral sites, yielding a spinel with cation distribution $(Li_{6/9}\square_{3/9})[Mn_{16/9}Li_{2/9}]O_4$, instead of $(Li_{8/9}\square_{1/9})[Mn_{16/9}\square_{2/9}]O_4$ in de Kock's formula. So it seems possible to prepare two Li–Mn–O spinels with *similar overall stoichiometry* $Li_2Mn_4O_9$, but *different vacancy distribution*. A comparison of their lithium intercalation properties is expected to be very interesting. Finally, the topotactic preparation of $Li_2Mn_4O_9$ by delithiation can, in principle, be achieved both chemically and electrochemically; both routes will be investigated here.

This paper describes the crystallographic and electrochemical properties of these "isomers," made by (1) de Kock's low-temperature solid state reaction procedure and (2) chemical and (3) electrochemical lithium extraction. While this work was in progress, an alternate route to $Li_2Mn_4O_9$ was published by Choi and Manthiram, using a lithium peroxide precursor (7). These authors made no attempt to determine the vacancy scheme of their spinel samples. Their results will be compared to ours herein.

2. EXPERIMENTAL

Samples *à la* de Kock (hereafter named "A") were made by solid state reaction between β-MnO_2 and LiOH at 400–500°C in air. For routes 2 and 3 above, the starting material was $Li_{1.22}Mn_{1.78}O_4$ powder (sample named "P" throughout this paper), which was prepared by solid state reaction from appropriate ratios of the same reagents at 600°C. Chemical delithiation was carried out by stirring 11 g of sample P in 0.1 M hydrochloric acid at room temperature for 20 hours (12). The sample was then filtered, washed with distilled water, and dried in air at 80°C. Electrochemical delithiation was made by a galvanostatic charge on sample P up to 4.30 V in a lithium cell. Samples obtained by chemical and electrochemical delithiation are named B and C, respectively.

Manganese oxidation states were determined by wet titrimetry using the oxalate–permanganate procedure, with at least three measurements per sample and an accuracy better than 1% (13). Quantitative elemental analysis of lithium (for sample B) and manganese was carried out on a Perkin-Elmer PA-360 atomic absorption spectrometer on samples dissolved in 2.5 M hydrochloric acid. The composition of sample B was determined from the combination of Li content, total Mn content, and oxidation state measurement; a detailed derivation of the formula from such anaytical data has been published by Feng *et al.* (14). The thermogravimetric behavior of samples B and P was determined on a Perkin-Elmer TGA-7 apparatus at heating rates in the range 0.5–4°C min^{-1} in dry oxygen.

X-ray diffraction characterization was carried out using a Siemens D-5000 diffractometer with Cu$K\alpha$ radiation. Neutron powder diffraction patterns were collected on the high-resolution two-axis D2B diffractometer at Institut Laue-Langevin, Grenoble, France, with a wavelength of 1.5938 Å on powder samples A and B loosely packed in vanadium cylindrical cans. This measurement could not be carried out on sample C because it requires sample quantities $\gtrsim$10 g. Structures were refined using the Rietveld method (*Fullprof* program (15)), using pseudo-Voigt profile functions.

For electrochemical studies, the active material was mixed with 20% carbon black and 10% PTFE emulsion. Cathodic pellets were cut from the resulting paste and dried under vacuum at 120°C for 15 hours before use. The electrolyte was 1 M $LiPF_6$ in EC-DMC (Merck), and the anode was lithium foil. Coin-type or Swagelok cells were assembled in a glove box with <1 ppm H_2O. Batteries were tested in either galvanostatic or potentiostatic mode at room temperature using a *MacPile* controller. Throughout this paper, all lithium intercalation levels x will refer to the normal spinel formula unit containing four oxygen atoms.

3. RESULTS AND DISCUSSION

3.1. Syntheses and X-Ray Diffraction

X-ray diffraction shows that all samples prepared have the spinel structure. Cell parameters and analytical data are given in Table 1. The solid state reaction procedure *à la* de Kock consistently yielded products containing traces of unreacted lithium carbonate and/or manganese dioxide, broad X-ray reflections, and a manganese oxidation state v(Mn) much lower than the theoretical value 4.0 expected for the ideal composition $Li_2Mn_4O_9$ (see values in Table 1).

TABLE 1
Preparation Conditions and Characterization of Samples

Sample	Synthesis procedure	Synthesis temperature (°C)	Analytical data			X-ray data	
			Li/Mn	v(Mn)	Formula	a (Å)	FWHM[a] (°2θ)
de Kock (4)	Solid state reaction	400	0.50[b]	n.d.[c]	$Li_{1-x}Mn_{2-2x}O_4$	8.162 (X-rays)	≈ 1.5[d]
Choi (7)	Via Li_2O_2 in aqueous medium	400	0.50[b]	3.77[e]	$Li_{0.94}Mn_{1.88}O_4$	8.107(28)	≈ 1.5[d]
A0	Solid state reaction	400	—	3.82[e]	$Li_{0.93}Mn_{1.86}O_4$	8.137(8)	1.35
A1	Solid state reaction	425	—	n.d.		8.153(9)	0.51
A2	Solid state reaction	500	—	3.69[e]	$Li_{0.95}Mn_{1.90}O_4$	8.179(3)	0.37
B	Chemical delithiation	25	0.23[e]	4.02[e]	$Li_{0.41}H_{0.45}Mn_{1.78}O_4$	8.091(2)	0.27
C	Electrochemical delithiation	25	0.50[e]	4.00[e]	$Li_{0.88}Mn_{1.78}O_4$	8.141(2)	0.32
P[f]	Solid state reaction	600	0.687[b]	3.81[b]	$Li_{1.22}Mn_{1.78}O_4$	8.163(2)	0.27

[a] Full width at half-maximum of 311 reflections.
[b] From overall stoichiometry.
[c] Not determined; 4.07 from neutron refinement of site occupations.
[d] Estimated from Fig. 2 in Ref. (4) and Fig. 1 in Ref. (7), respectively.
[e] From chemical or electrochemical analysis.
[f] Stoichiometric spinel $Li_{11/9}Mn_{16/9}O_4$; parent compound of B and C.

A considerable decrease in both unreacted reagents' content and spinel reflections linewidths could be achieved by increasing the reaction temperature, as shown in Fig. 2. However, this process also decreased v(Mn), thus bringing the composition even farther from the ideal one. Despite this low manganese valence, the cell parameter of sample A2 agrees well with that reported by de Kock *et al.* (4), but it is significantly higher that those observed on A0–A1 and on delithiated samples B and C. This is consistent with a lower v(Mn) in sample A2 and again in disagreement with the ideal formula $Li_2Mn_4O_9$. Samples prepared by the hydrogen peroxide route in a similar temperature range also exhibit broad X-ray reflections (7). In that case, an increase in synthesis temperature resulted in a decrease in X-ray linewidths, but also in the formation of Mn_2O_3 impurity above 450°C. The cell parameter value reported for the 400°C sample is very low and determined with a high uncertainty (see Table 1), possibly indicating a particular cation/vacancy distribution.

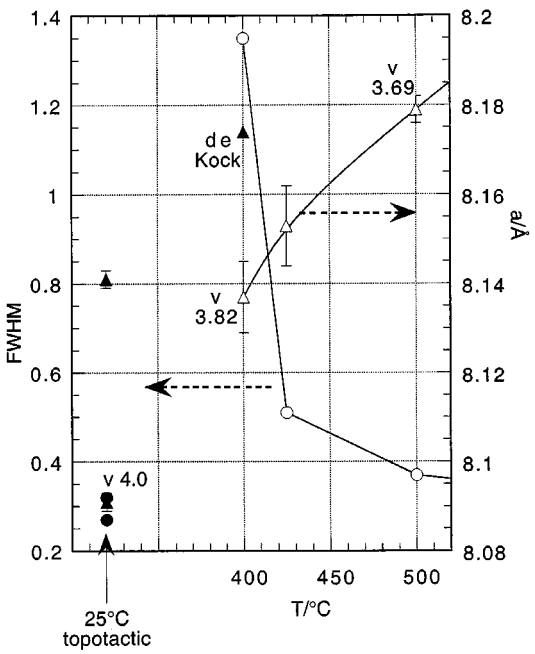

FIG. 2. Evolution of spinel cell parameter a, 311-reflection full width at half-maximum ($FWHM$), and Mn oxidation state as a function of reaction temperature.

For the topotactic synthesis of sample C by electrochemical delithiation, the reaction progress can be followed by the voltage profile in the lithium cell used, starting with composition P as the positive electrode. This curve (see Fig. 3) shows a voltage plateau at ca. 4.1 V, which is typical of lithium extraction from the tetrahedral spinel sites (1). The capacity expected for $Li_{1.22}Mn_{1.78}O_4$ up to the limit v(Mn) $= 4$ (0.33 Li extracted per formula unit) is reached at $\approx$4.25 V, and this limit shows up as the onset of a domain with a steeper potential increase in the chronopotentiometric curve (Fig. 3).

Sample B gave the cleanest X-ray diffraction pattern, with no line broadening with respect to its parent compound P and an experimental v(Mn) value equal to 4.0 within experimental errors. But it also yielded a much lower lithium content than expected (Li/Mn = 0.23, see Table 1). This result can be explained taking into account the possibility of proton exchange for lithium during acidic treatment. Several studies (14, 16) showed indeed that acidic treatment of $Li_{1+\alpha}Mn_{2-\alpha}O_4$ spinels gives rise to an increasing exchange of Li^+ by protons with increasing manganese valence, i.e.,

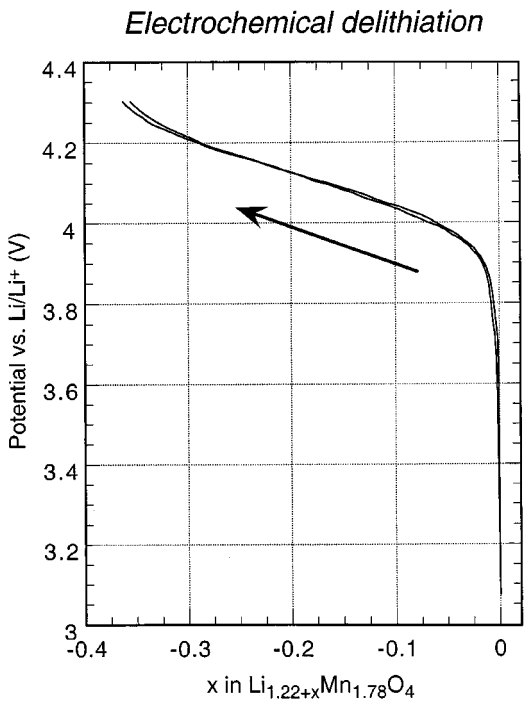

FIG. 3. Evolution of cell voltage as a function of lithium content during room-temperature electrochemical delithiation from $Li_{1.22}Mn_{1.78}O_4$ (two cells shown).

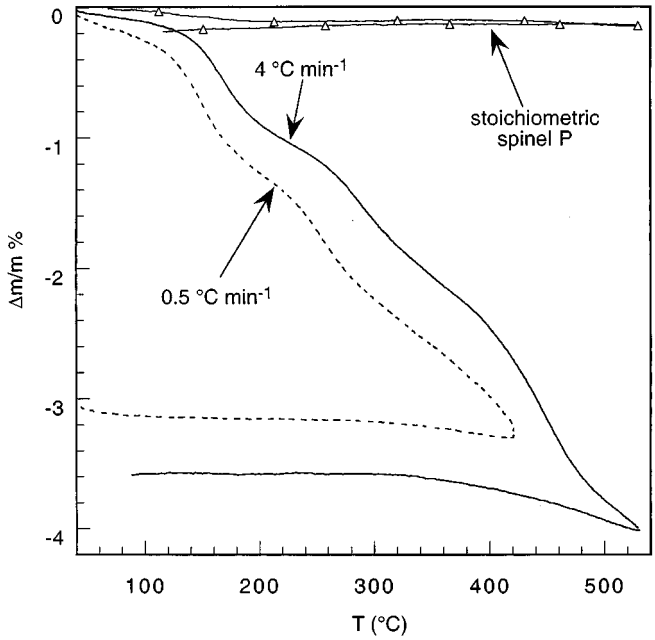

FIG. 4. Thermogravimetric analysis in oxygen of sample B, obtained by chemical delithiation from stoichiometric spinel P ($Li_{1.22}Mn_{1.78}O_4$). The TG trace of sample P is shown at the top (thin line with triangle marks).

with increasing α value. Analytical data give a composition $Li_{0.41}H_{\approx 0.45}Mn_{1.78}O_4$ (or $Li_{0.92}HMn_4O_9$), i.e., a vacant spinel with partial replacement of Li^+ by H^+. These formulas are in good agreement with the ratio of lithium lost by oxidative extraction and by proton exchange expected as a function of manganese valence from previous studies (14).

The difference in cell parameter between samples B and C, obtained by chemical or electrochemical delithiation (see Table 1), can be explained by this major difference in composition. Whereas the manganese valence is the same between samples B and C, an important fraction of lithium has been replaced by protons in the former, resulting in a significantly smaller cell parameter.

3.2. *Thermogravimetric Analysis*

The presence of protons was confirmed by thermogravimetry (TG). The thermal stabilities of the stoichiometric spinel P and sample B are compared in Fig. 4. While the former shows a negligible mass change up to 500°C in oxygen, the acid-treated sample B undergoes a continuous mass loss starting at ca. 120°C. This feature is irreversible and probably results from a succession of several steps as a function of temperature, as shown by slope changes in Fig. 4. Unfortunately, these steps are poorly separated, even at low heating rate (0.5°C min^{-1}, see dotted line in Fig. 4). Possible causes for mass losses in this sample are (i) the presence of protons, as hydratation molecules or hydroxyl groups, (ii) structural rearrangements due the presence of vacancies, and (iii) reduction of tetravalent manganese. This last factor prompted us to perform the TG measurements in oxygen, with the intent to delay reductive decomposition reactions. Experimental results show that at 350°C in oxygen, this proton-containing, lacunar spinel is already decomposed to β-MnO_2 and a spinel phase with higher cell parameter, i.e., higher lithium content ($a = 8.147$ Å, compared to 8.091 Å for sample B).

The composition obtained in Section 3.1. for sample B yields a mass loss of 2.73% for the departure of protons (as water). This corresponds to a temperature of 350°C in the slow-heating TG curve in Fig. 4, showing that protons are strongly bonded in spinel B. In addition, the mass loss is very small below 120°C, further confirming that protons are not present as adsorbed water. These results are consistent with Feng's study (14), in which it was concluded that the mass loss up to ca. 300°C was due to protons introduced by ion exchange in acid-treated $Li_{1+\alpha}Mn_{2-\alpha}O_4$ spinels.

3.3. *Neutron Diffraction*

Final Rietveld refinements from neutron diffraction data included the following variables: (i) global parameters: zero-shift correction, four to six background polynomial coefficients, (ii) profile parameters for the spinel phase: scale

factor, unit cell parameter, four profile parameters for the pseudo-Voigt function, (iii) structural parameters: oxygen position parameter, isotropic displacement coefficients B_{iso} for manganese and oxygen sites, occupancies of all sites but oxygen. B_{iso} could not be refined for lithium, because a strong correlation with site occupancy resulted in unreasonably large standard deviations. It was thus fixed to 1.50 $Å^2$; a test with a value of 1.0 showed an effect of less than 4% on the 8*a* site occupancy. For sample A2, a β-MnO_2 phase was included, with the same profile parameters as those for the main spinel phase, and only cell parameters refined. For sample B, both lithium and manganese were placed on octahedral 16*d* sites and varied independently. This strategy resulted in 17 and 20 variables for samples A2 and B, respectively. Observed and calculated neutron diffraction patterns and refinement parameters are given in Fig. 5 and Table 2, respectively.

Samples of the A series yielded broad neutron diffraction peaks, just as already noted for X rays. This, together with the presence of unreacted starting materials, precluded any satisfactory refinement for sample A1 (prepared at 425°C). The 500°C sample A2 could be refined, taking into account the weak lines of β-MnO_2. Its neutron diffraction diagram also showed a broad hump centered at 43.3° 2θ (also present in sample B, see Figs. 5a and 5b). The origin of this feature is not known; the 42–44° range, which does not include any spinel reflection, was excluded from the refinement. Results are summarized in Table 2. The large linewidths made the profile difficult to fit and resulted in somewhat high R_p and R_{wp} values. The possibility of finding lithium on octahedral 16*d* sites was tested and found negligible. Our refinement (see Table 2) confirms the double vacancy scheme proposed by de Kock *et al.* (4). But the composition of A2 deviates significantly from the ideal $Li_2Mn_4O_9$ formula, yielding vacancy fractions larger on tetrahedral sites (as was already the case in Ref. (4)) and smaller on octahedral sites. This results in a calculated Mn valence of 3.83 in the spinel phase, still quite far from the ideal 4.00 value for $Li_2Mn_4O_9$.

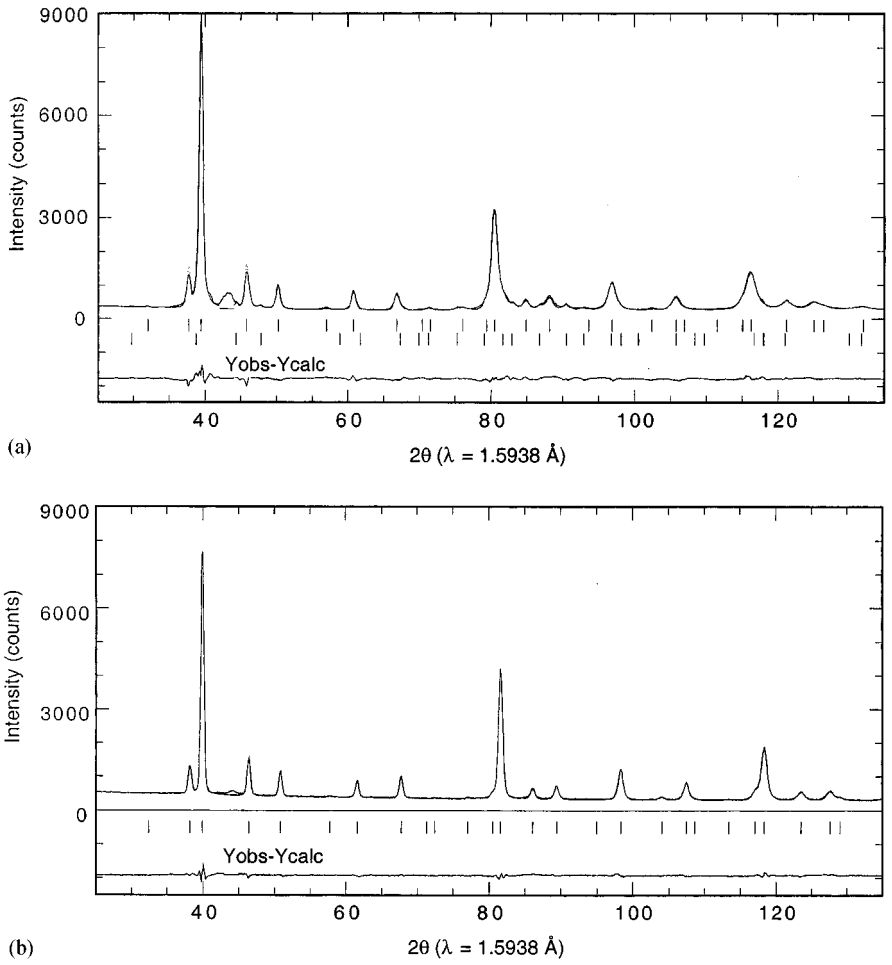

FIG. 5. Observed (points) and calculated (continuous line) neutron powder patterns of samples A2 (from solid state reaction *à la* de Kock) and B (from chemical lithium extraction). Differences I_{obs}–I_{calc} are shown at the bottom.

TABLE 2
Results of Rietveld Refinements from Neutron Diffraction Data: Spinel Structure, Space Group $Fd\bar{3}m$, $x = y = z$ for All Sites

Cell parameters (Å)	Atom	Site	x, y, z	Site Occupancy	B_{iso} (Å^2)	Refinement parameters
			Sample A2			
			(two-phase refinement including β-MnO_2)			
Spinel:	Li	8*a*	0.125	0.78(2)	1.5	N − P + C 2441
8.1811(3)	Mn	16*d*	0.5	0.94(1)	1.38(6)	$R_p = 4.37$, $R_{wp} = 5.76$
	O	32*e*	0.26352(5)	1	1.17(3)	$R_{exp} = 1.61$, $R_{Bragg} = 4.68$
β-MnO_2:						35 spinel reflections used
$a = 4.3955(8)$						
$b = 2.875(1)$						
			Formula for sample A2: $(Li_{0.78}\square_{0.22})[Mn_{1.88}\square_{0.12}]\ O_4$			
			According to Ref. (4): $(Li_{0.83}\square_{0.17})[Mn_{1.76}\square_{0.24}]\ O_4$			
			Theor. for $Li_2Mn_4O_9$: $(Li_{0.89}\square_{0.11})\ [Mn_{1.78}\square_{0.22}]\ O_4$			
			Sample B			
8.0916(2)	Li1	8*a*	0.125	0.23(2)	1.5	N − P + C 2438
	H	32*e*	0.1520(9)[a]	0.076(6)	1.5	$R_p = 2.47$, $R_{wp} = 3.18$
	Li2	16*d*	0.5	0.095(11)	0.58(3)	$R_{exp} = 1.68$, $R_{Bragg} = 5.12$
	Mn	16*d*	0.5	0.905(11)	0.58(3)	33 spinel reflections used
	O	32*e*	0.26261(3)	1	0.67(2)	
			Formula for sample B: $(Li_{0.23}H_{0.30}\square_{0.58})[Mn_{1.81}Li_{0.19}]O_4$			
			From chemical analysis: $(Li_{0.19}H_{0.45}\square_{0.64})[Mn_{1.78}Li_{0.22}]O_4$			

[a] Not refined simultaneously with Li and H occupancies (see text).

The presence of protons in sample B was confirmed by a significantly higher background, due to incoherent hydrogen scattering. In a first step, the structure was refined with lithium, manganese, and oxygen atoms only. Several proton sites located along O–O lines in the spinel structure were proposed previously for the formation of strong OH bonds on the basis of infrared spectroscopy data (17). Tests for all these yielded negative or negligible hydrogen occupations. A direct replacement of Li by H on the tetragonal 8*a* site was also ruled out because of an unreasonable 8*a*–O length for an O–H bond (18). Using Fourier difference maps, we found a possible proton site near 8*a*, but significantly shifted from the center of the (8*a*–O_4) tetrahedron toward one oxygen atom. Refinements showed that this site could be described by a 32*e* position (x, x, x) with $x = 0.152$. Strong correlations between this position parameter and Li1 and H occupancies did not allow an independent refinement of these three variables. It was thus decided to proceed in two steps, refining (1) x(H) with occupancies fixed according to the analytical stoichiometry and (2) the Li1 and H occupancies with this x(H) fixed. Additional attempts to place H in a neighbouring 96 g site as proposed in Ref. (19) led to a poorer refinement. Results (see Table 2, lower part) show a fairly good agreement with the chemical formula, given the e.s.d. on occupancies from neutron data. A remarkable result is the negliglible shift in composition on the 16*d* site after acidic treatment in sample B. No vacancies were found on this site (independent refinements of Mn and Li occupancies on this site led to a total occupancy of 0.999). In contrast, the occupations of both Li1 (8*a*) and H sites are low, allowing the protons to occupy 32*e* sites adjacent to unoccupied lithium 8*a* sites. Mn–O and Li–O distances are given in Table 3. The experimental O–H bond length in sample B is 1.5642(3) Å.

This refinement confirms that an acid treatment on a $Li_{1+\alpha}Mn_{2-\alpha}O_4$ spinel (i) induces a partial exchange Li^+–H^+, (ii) has a negligible effect on the octahedral site content, and (iii) yields a spinel phase containing an important fraction of vacancies on the 8*a* site.

The compositions of samples A2 and B, together with those of relevant nonvacant Li–Mn–O spinels studied by neutron diffraction, are shown in the phase diagram in Fig. 6. Li–O and Mn–O distances calculated from neutron data are compared in Table 3. The experimental Mn–O distances are 0.01–0.02 Å smaller than expected from Shannon's ionic radii (18) (see Table 3, last column). Figure 6 shows that the variation in spinel cell parameters and Mn–O bond lengths can be accounted for by two main parameters: (i) the oxidation state of manganese, governing the bond length decrease along the $LiMn_2O_4$–MnO_2 delithiation line and in the $LiMn_2O_4$–A2–B series, and (ii) the occupation of the B site. The availability of samples B and C allows us, for the first time, to place three points on an almost horizontal line in the diagram (dash-dotted line $Li_xMn_2O_4$–$Li_4Mn_5O_{12}$ in Fig. 6), unambiguously showing that the octahedral cation–oxygen distance d_{B-O} increases with increasing lithium fraction on this site at constant manganese valence. This bond length also increases with the

TABLE 3
Cation–Anion Distances in Selected Li–Mn–O Spinels As Determined from Neutron Diffraction Data (A = Tetrahedral Site, B = Octahedral Site)

Composition	v(Mn)[a]	Cell Parameter (Å)	x(O)	d_{B-O}, exp. (Å)	d_{A-O}, exp. (Å)	Ref.	$\langle d_{B-O}\rangle$ Shannon[b] (Å)
$LiMn_2O_4$	3.506	8.2449	0.2632	1.9584(4)	1.9736(4)	15	1.985
$Li_{0.19}Mn_2O_4$ ($\approx$ "λ-MnO_2")	3.905	8.0215	0.2626	1.9097	1.9118	16	1.94
$Li_{1.34}Mn_{1.66}O_4$ ($\approx Li_4Mn_5O_{12}$)	4.01	8.1407	0.2630	1.935	1.9456	17	1.97
$Li_{0.83}Mn_{1.76}O_4$	4.07	8.174	0.2634	1.938	1.958	4	1.94
$Li_{0.79}Mn_{1.88}O_4$	3.83	8.180	0.2634	1.9416(6)	1.9613(6)	This work (sample A2)	1.957
$Li_{0.40}H_{\approx 0.5}Mn_{1.78}O_4$	4.02	8.091	0.2626	1.9263(3)	1.9286(3)	This work (sample B)	1.962

[a] From stoichiometry obtained by refinement of site occupations from neutron diffraction data.
[b] Calculated average 16d cation–oxygen distance according to cation radii from Ref. (18).

presence of vacancies on the octahedral site (case of sample B). The cell parameter and bond length calculated from de Kock's data (4) further confirm that their "$Li_2Mn_4O_9$" sample (marked with "?" in Fig. 6) probably lies close to the A2 composition in the phase diagram.

3.4. Electrochemical Properties

Li–Mn–O spinels undergo lithium insertion/extraction at either 4 V (8a sites) or 3 V (filling additional lithium sites) vs Li/Li^+ couple. The former reaction is limited by the manganese valence v(Mn), which cannot exceed 4. The latter is usually considered less interesting for applications, because it corresponds to a lower v(Mn) range (between 3 and 3.5 when starting from $LiMn_2O_4$), where extensive Jahn–Teller distortion occurs. This phenomenon is an intrinsic property of the Mn^{3+} ion ($t_{2g}^3e_g^1$ electronic configuration) and is very deleterious to reversibility of intercalation reactions (1). The electrochemical interest of cation-vacant Li–Mn–O spinels is two-fold:

(i) they have v(Mn) close to $+4$, and can be expected to intercalate lithium (3 V reaction) while staying away from the Jahn–Teller distorsion limit v(Mn) = 3.5, unlike $LiMn_2O_4$;

(ii) an extra intercalation capacity is expected to occur because of lithium vacancies, and might show up as distinct steps in charge–discharge curves.

In addition, since samples A, B, and C have a fraction of vacant tetrahedral 8a sites, a significant initial lithium intercalation capacity is expected to occur at 4 V vs Li/Li^+. A comparison of first discharges (Fig. 7) shows that this high-potential capacity fraction is observed only on sample C, which is actually prepared *in situ* by a preliminary charge

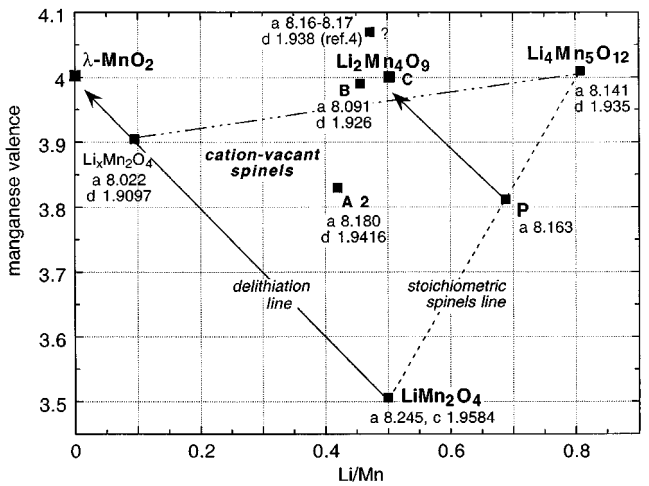

FIG. 6. Composition–valence phase diagram for the Li–Mn–O system, showing the actual stoichiometry of samples and delithiation lines (arrows). The actual abscissa for sample B is (Li + H)/Mn. Numbers indicate cell parameters a and Mn–O bond lengths d as calculated from neutron diffraction data (both in angstroms). See Table 3 for references.

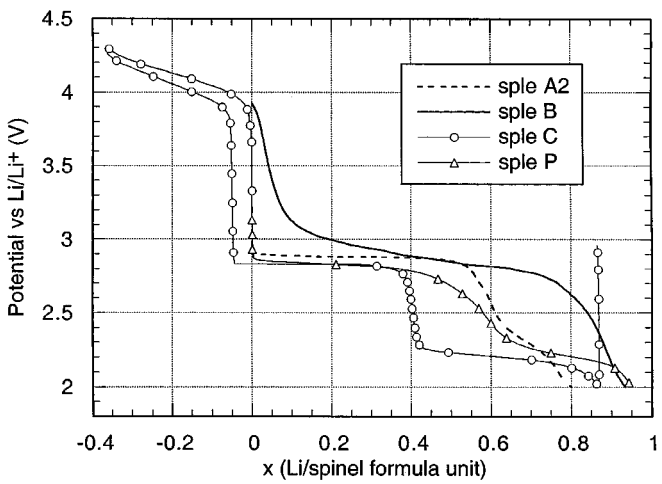

FIG. 7. First discharge at slow rate ($\leq C/50$) of samples A2, B, C, and P. The origin of the step down to 2.2 V, especially prominent for sample C, is kinetic, as evidenced by the return of potential to 2.9 V on relaxation at the end of discharge.

(delithiation). Sample B has a fairly high initial potential (3.92 ± 0.05 V), but this decreases rapidly at the beginning of discharge and the capacity above 3.5 V is <0.05 Li per spinel formula unit, i.e., much less than expected for a compound containing 0.38 tetrahedral vacancies. Sample A2 behaves like a normal, nondeficient spinel with an initial potential of ca. 3.2 V and an immediate drop to the voltage plateau at 2.9 V on discharge. A similar behavior was observed by de Kock *et al.* on "$Li_2Mn_4O_9$" (4).

Details of the first electrochemical cycle were studied by slow-scanning voltammetry (10 mV/h), as shown in Fig. 8, where stoichiometric $LiMn_2O_4$ is included as a reference. It shows clear characteristics of a two-phase system in all cases (common origin of reduction and oxidation peaks (20)). Compounds A2, B, and P have a similar equilibrium potential for this two-phase redox reaction, obtained by interpolation between reduction and oxidation peak onsets. Its value is slightly lower than that of $LiMn_2O_4$ (2.90 and 2.96 V, respectively).

These voltammograms also reveal a particular feature of sample B: the presence of a separate redox step occurring ca. 200 mV above the main charge/discharge step (see asterisks in Fig. 8). This result is remarkable in several ways: (i) this feature is observed neither on the parent stoichiometric compound P, nor on the electrochemically delithiated sample C; (ii) it is *reversible* and remains stable on cycling, as shown in Fig. 9b, which displays 20 charge–discharge cycles on this material. The associated capacity is ≈ 0.20 Li per formula, i.e., equal to the *B* site lithium fraction in sample B.

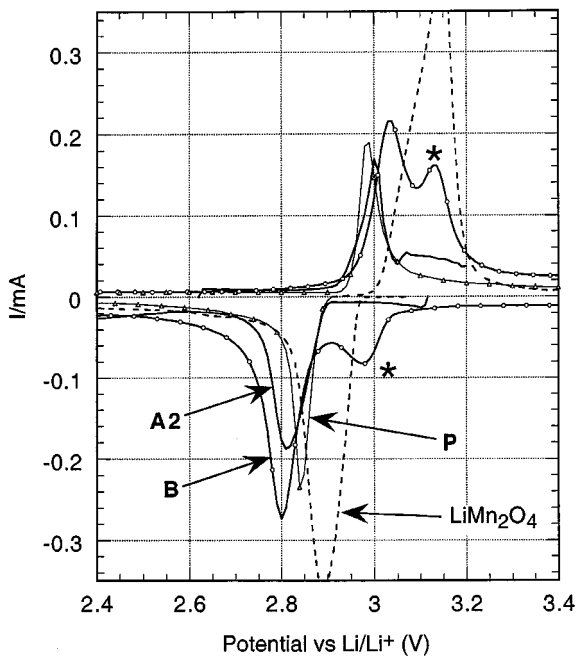

FIG. 8. Slow step scanning voltammetry of samples A2, B, and P at 10 mV/h.

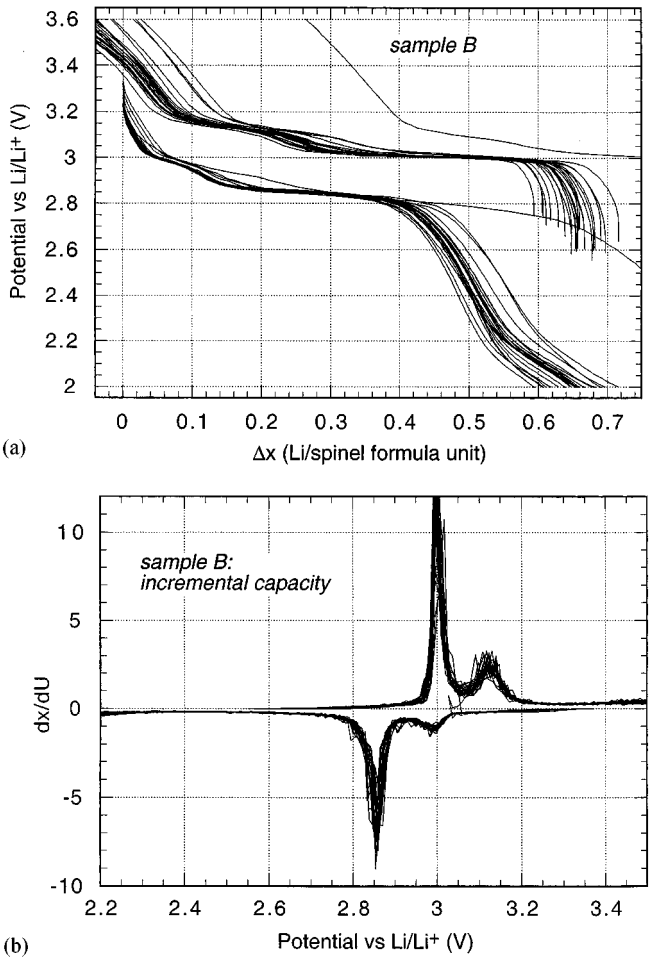

FIG. 9. Galvanostatic cycling of sample B at C/20 rate (top); corresponding incremental capacity curve (bottom). Twenty cycles are shown.

Given the fact that B gives the sharpest X-ray reflections among cation-deficient samples, a possible explanation for this is *B* site Li/Mn ordering. Intercalation sites surrounded by Li-occupied *B* sites would give rise to lower electrostatic repulsion, and consequently to a preferential occupation by intercalated cations occuring at a lower reducing potential than sites adjacent to $Mn^{3+/4+}$ cations. However, given the low scattering power of lithium, no experimental confirmation of such an ordering could be found. Another possible explanation for this extra step, the formation of a fraction of ramsdellite-type MnO_2 as a result of the acid treatment (21), can be ruled out on the basis of X rays and neutron data.

Galvanostatic cyclings at $\approx C/10$ rate show that samples A2 and B are both very stable on cycling in the potential window 2.0–3.6 V (see Figs. 9 and 10). The differential capacity curves illustrate the main differences between these two intercalation hosts: a flatter voltage plateau, i.e., sharper current peaks for A2, and the additional step starting at 3.10 V for B. Initial capacities are slightly higher for the

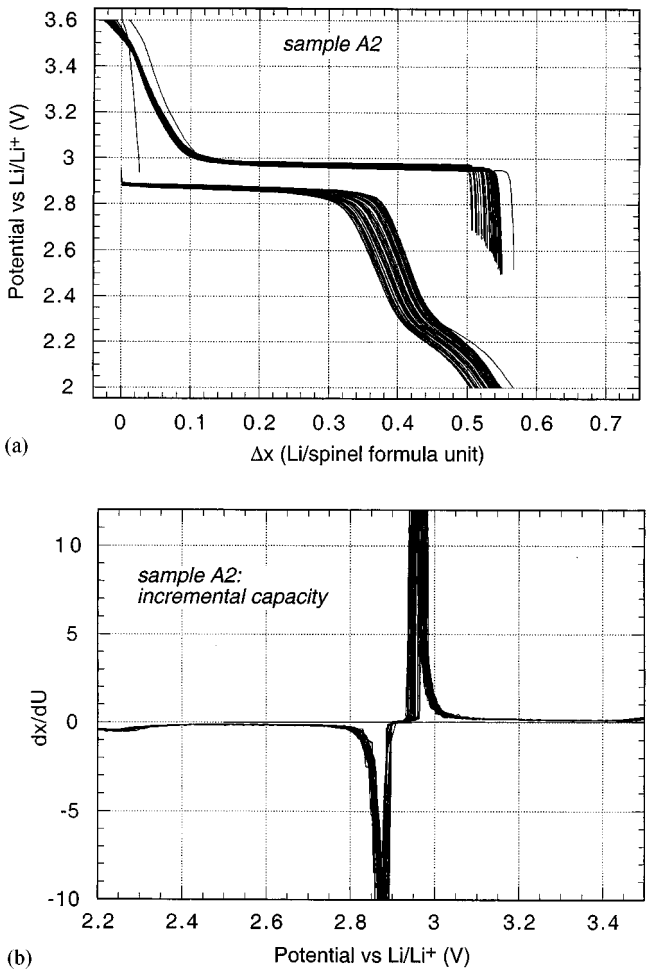

FIG. 10. Same as Fig. 8 for sample A2 at $C/10$ rate.

latter, as expected from its higher initial manganese oxidation state. Figure 11 shows that their performances level out after ca. 30 cycles, and that both cation-vacant spinels are much more stable than stoichiometric $LiMn_2O_4$. The double-vacancy sample A2 is especially stable, and maintains a capacity of 0.5 Li, corresponding to 80 mAh/g, at the 85th cycle. We note that this capacity 0.5 Li corresponds to a lower limit of manganese oxidation state equal to $+3.5$, i.e., the limiting Mn^{3+} fraction above which a cooperative Jahn–Teller occurs, leading to a structural distortion (1). Analysis of A2 and B electrochemical cells stopped after cycling indeed did not reveal any significant tetragonal distortion in these materials. Average cell parameters obtained on oxide samples from cells stopped in discharged state yielded 8.183 and 8.171 Å for samples A2 and B, respectively. The remarkably small volume change in the A2 case ($\Delta a = 0.004$ Å) may be a major factor in the superior stability of this material after more than 80 charge–discharge cycles. In a slightly wider potential window, high cycling capacities were also reported up to the 30th cycle for

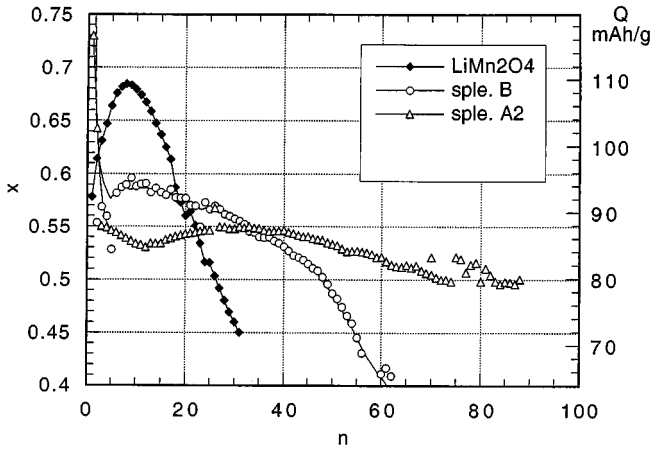

FIG. 11. Evolution of the 3-V capacity on cycling at $\approx C/10$: cell 54 = stoichiometric $LiMn_2O_4$, cell 55 = sample B (tetrahedral-vacancy spinel), cell 56 = sample A2 (double-vacancy spinel).

$Li_4Mn_5O_{12}$-like samples prepared from lithium peroxide at 400°C (7). Our results confirm the superior stability of such vacancy-containing Li–Mn–O spinels with high initial manganese valence and partial disorder as shown by the large linewidth of X-ray and neutron reflections.

4. CONCLUSIONS

This study allowed us to confirm the double-vacancy scheme for Li–Mn–O spinels prepared by low-temperature solid state reaction. It also showed remarkable differences between spinel-type compounds with compositions close to $Li_2Mn_4O_9$, depending on the distribution of cationic vacancies and inclusion of protons in the lattice. This difference also shows in their electrochemical behavior in lithium batteries: whereas the capacity associated with vacancy filling is barely noticeable in the double-vacancy compound A2, an extra lithium insertion/extraction step is clearly visible in sample B obtained by room-temperature chemical delithiation. Both compounds are much more stable than stoichiometric $LiMn_2O_4$ on cycling in the 3 V region; however, the main advantage of these materials in terms of electrochemical stability does not directly result from lithium intercalation into cation vacancies, but rather from their higher initial manganese oxidation state and exceptionally small cell expansion in the case of the double-vacancy spinel B.

ACKNOWLEDGMENTS

A.I.'s work is supported by a Ph.D. grant from the Mexican–French cooperation program Conacyt. We thank Institut Laue-Langevin for the use of the D2B diffractometer, E. Suard for her assistance at ILL, and F. Le Cras for his contribution in the preparation of several samples.

REFERENCES

1. M. M. Thackeray, *J. Electrochem. Soc.* **142,** 2558 (1995).
2. F. Le Cras, P. Strobel, M. Anne, D. Bloch, J. B. Soupart, and J. C. Rousche, *Eur. J. Solid State Inorg. Chem.* **33,** 67 (1996).
3. J. M. Paulsen and J. R. Dahn, *Chem. Mater.* **11,** 3065 (1999).
4. A. de Kock, M. H. Rossouw, L. A. de Picciotto, and M. M. Thackeray, *Mater. Res. Bull.* **25,** 657 (1990).
5. F. Le Cras, Ph.D. thesis, Grenoble, 1996.
6. C. Masquelier, private communication.
7. S. Choi and A. Manthiram, *J. Electrochem. Soc.* **147,** 1623 (2000).
8. G. X. Wang, S. Zhong, D. H. Bradhurst, S. X. Dou, and H. K. Liu, *J. Power Sources* **74,** 198 (1998).
9. Y. J. Lee, F. Wang, and C. P. Grey, *J. Amer. Chem. Soc.* **120,** 12601 (1998).
10. R. Kostecki, F. Kong, Y. Matsuo, and F. McLarnon, *Electrochem. Acta* **45,** 225 (1999).
11. P. Strobel, F. Le Cras, M. Anne, and D. Bloch, *J. Solid State Chem.* **124,** 83 (1996).
12. J. C. Hunter, *J. Solid State Chem.* **39,** 142 (1981).
13. G. Charlot, "Chimie Analytique Quantitative", Vol. II, p. 442. Masson, Paris, 1974.
14. Q. Feng, Y. Miyai, H. Kanoh, and K. Ooi, *Langmuir* **8,** 1861 (1992).
15. J. Rodrigez-Carvajal, *Physica B* **192,** 55 (1993).
16. P. Lavela, L. Sanchez, J. L. Tirado, S. Bach, and J. L. Pereira-Ramos, *J. Solid State Chem.* **150,** 196 (2000).
17. B. Ammundsen, D. J. Jones, J. Rozière, and G. R. Burns, *Chem. Mater.* **7,** 2151 (1995).
18. R. D. Shannon, *Acta Crystallogr.* **32,** 751 (1976).
19. B. Ammundsen, D. J. Jones, J. Rozière, H. Berg, R. Tellgren, and J. O. Thomas, *Chem. Mater.* **10,** 1680 (1998).
20. Y. Chabre, *in* "Chemical Physics of Intercalation II" (P. Bernier, Ed.), p. 181. Plenum, New York, 1993.
21. D. Larcher, P. Courjal, R. Herrera, B. Gérand, A. Blyr, A. du Pasquier, and J. M. Tarascon, *J. Electrochem. Soc.* **145,** 3392 (1998).